pixels are due to NeuroQuant blending colors between adjacent regions. These were ignored. A surface rendering of the final volume is shown in Figure 7.

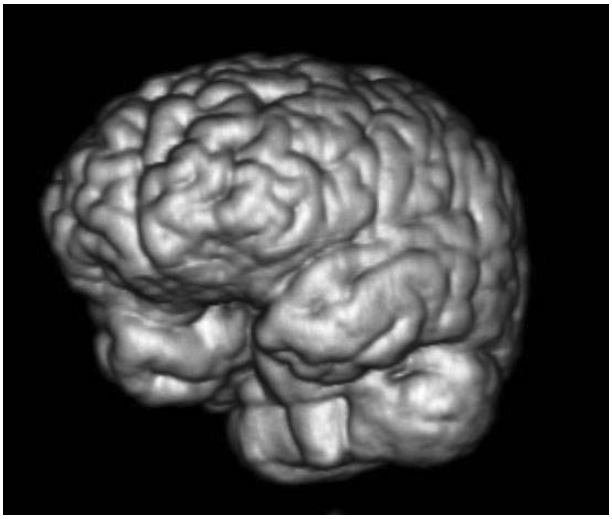

Figure 7. Surface rendering of the final volume

(3) Assigning appropriate values to segmented regions

To assign value to the PET image we evaluated amyloid positive PET images obtained at UW (Figure 8) and reviewed with a Nuclear Medicine physician (David Lewis, MD) trained in evaluation of such images. The ratio of grey matter in the cerebral cortex to the cerebellum is termed SUVr. Normal values of SUVr are typically 1.2, abnormal values are 1.67, and a proposed threshold between normal and abnormal in 1.4.

In addition, amyloid positive PET images loose the distinction between grey and white matter in the cerebral cortex, due to the increased uptake of amyloid tracer in the grey matter (Figure 8).

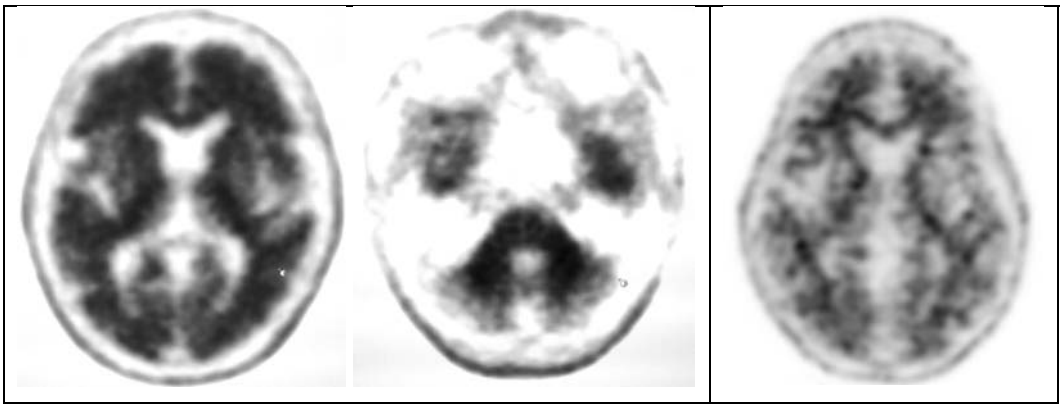

Figure 8. Left: Midbrain- and cerebellum-level sections of an amyloid-positive PET image of a patient. Right: Midbrain-level section of an amyloid-negative PET image of a patient showing decreased relative uptake in grey matter region.

Based on these considerations we set the SUVr to 1.67. It should be noted however that the appropriate level may be dependent on several factors, including choice of tracer (there are now several), scan timing, ROI definition, and image reconstruction methods.

(4) Adding plausible levels of blurring and noise

Uncorrelated Poisson noise was then added to each voxel and a 3D Gaussian smoothing was performed with a 6 mm FWHM. The noise level was decided by visual comparison to a patient image. The result is shown in Figure 9.

For comparison, Figure 10 shows a composite set of sections through an image of the physical phantom. There are differences in the layout due to the design and machining process, and water from the phantom body leaked back into the fill reservoir, resulting in a limited amount of draining of the phantom body back into the fill reservoir. This lead to a reduction in activity in the frontal area of the cortex, as well as the frontal area of the cerebellum, in an otherwise successful first phantom imaging experiment. Importantly, the overall similarity to the DRO in Figure 9 is apparent, even though the image section locations do not match. Full details of the physical phantom development, construction, and imaging are given in the companion report by John Sunderland.

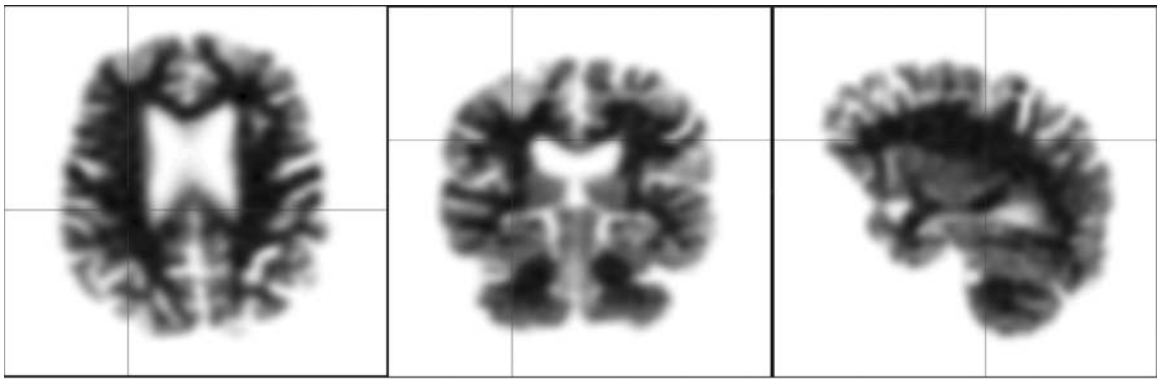

Figure 9. Sections through the first version of the PET amyloid tracer digital reference object (DRO).

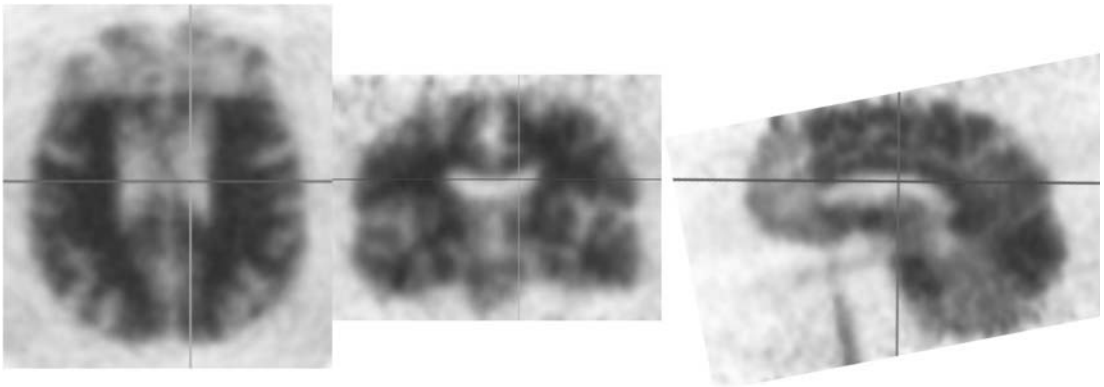

Figure 10. Siemens HR+ PET scans of the physical phantom. Draining of activity from compartments in the frontal area of the brain is apparent, but overall similarity to the DRO is apparent.

(5) Saving the DRO in a DICOM structure

We used the methodology developed for the original FDG-PET/CT DRO. We used the open-source DICOM software (DICOM Toolkit; Offis, Oldenberg, Germany) to create the PET DICOM files that contains the image volume. The DICOM file headers were populated with only the minimal information required by the DICOM standards for whole-body static PET imaging.

PET DICOM files were then subjected to validation and verification tests by using the DICOM validation software (dicom3tools; http://www. dclunie.com) to verify the DICOM file structure and conformance. A final inspection of the header fields was performed by manually reading each field from three of the DICOM files and verifying the correct DICOM field values, lengths, and associated DICOM types.

Evaluation

We requested evaluation of the amyloid-PET DRO by members of the QIBA Amyloid PET Biomarker Committee, as we received a total of four careful evaluations: John Sunderland (U Iowa), Anne Smith (Siemens), Dawn Matthews (ADM Diagnostics, LLC), and Greg Klein (BioClinica, Inc.). In addition we requested a review from a Nuclear Medicine physician (David Lewis, MD) trained in evaluation of such images.

Here is a summary of the findings:

(1) All of the reviewers noted that visually the images looked realistic and that the DRO has great potential. In addition the connection with the physical phantom (Figure 10) is important.

(2) Phantom orientation: All of the reviewers noted that the image was not properly oriented, with the sagittal and coronal images upside down.

(3) Greg Klein noted the alignment: "Ideally, we recommend that amyloid images be acquired using axial alignment to the orbital-metal plane. These are tilted pretty far from that. Could that be fixed?"

(4) Artifact: All of the reviewers noted a transverse artifact as shown below (Figure 11 courtesy of Anne Smith). This turned out to be a failure of the segmentation algorithm on two slices, and is readily correctable.

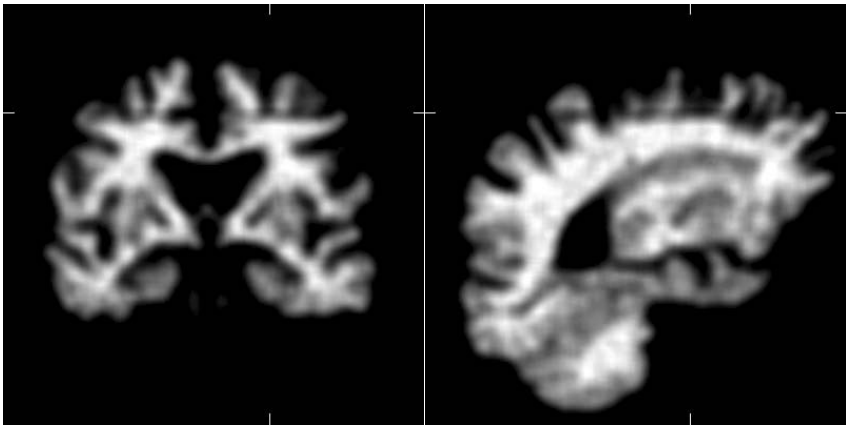

Figure 11. Image of the DRO from ASIPro.

(5) Anne Smith was unable to load the images properly.

" I am unable to load the 256 slice dataset into our Siemens 3D viewers (TrueD and the 3D Taskcard on the scanner consoles). I can load it into our 2D Viewing taskcard, but even there, it does not load as expected. Normally a 3D image will display with 4 slices on the screen at a time (the default layout). However, this dataset will only display in one of the panes, the other 3 appear empty. I can scroll through the dataset but I can only see one plane on the screen at a time.

I was able to load the dataset into ASIPro, my IDL-based small animal imaging viewer that uses the Merge libraries for DICOM."

(6) All of the reviewers noted that it would be valuable to have the MRI (and potentially CT) images of the phantom as well. This was for several reasons, including workflow and for analysis and understanding.

(7) A variety of software packages that would be used for analysis were listed, including, but not limited to, the Siemens Scenium package, the PETMAX software from ADM Diagnostics, PMOD, and others. An image from PMOD (Figure 12 courtesy of Greg Klein) is shown below

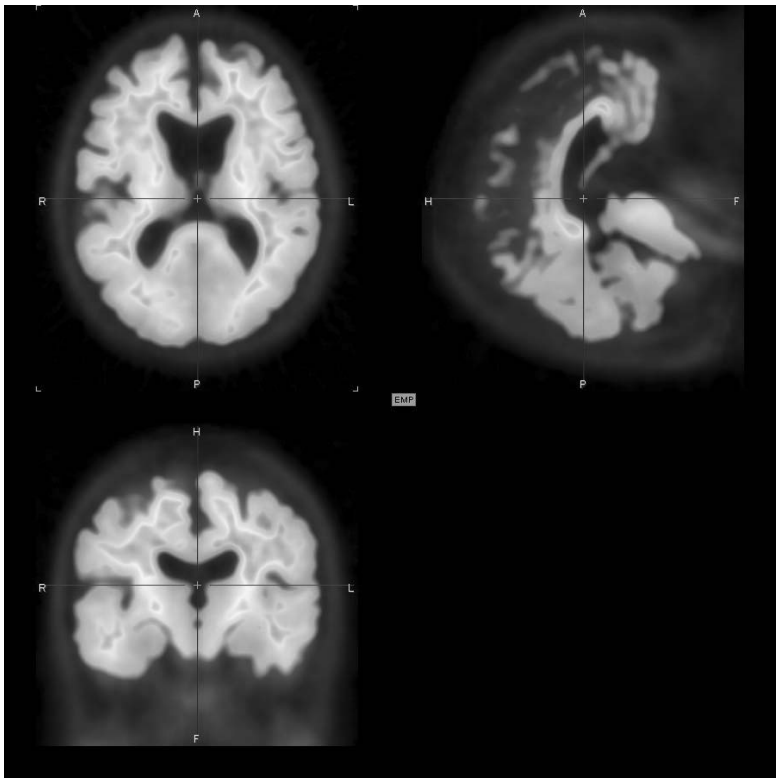

Figure 12 Image of the DRO from PMOD.

(8) Image values and ratios: Greg Klein noted that

"... Visually, it's a pretty strong "normal" amyloid negative case. I computed a quick PET-only SUVR using Avid's "Clark JAMA2011" method, and get a composite SUVR referenced to whole cerebellum equal to 0.87. That's a pretty strong amyloid negative compared to the cutpoint for this method, which for Amyvid would be set to about 1.1. Are you also considering a more positive amyloid case as well? If we're going with a single phantom for amyloid, then probably best to have one with

good grey/white contrast like this one so that you can verify visually that a scanner can resolve this sufficiently. After all, in an amyloid positive case where grey and white matter have roughly equal uptake, there isn't much to resolve!"

Dawn Mathews noted that

"If positivity is determined through SUVR calculations, then it is important to identify the intended SUVR thresholds when using the pons and whole cerebellum as references. As mentioned in my previous notes, the intensities did not seem consistent with typical florbetapir scans but this may have been by design, so a translation guide would be important.

One reason I used a high intensity in the images was to test whether the true negative florbetapir scan would show any expansion of white matter under those conditions, and to bring out any possible phantom "positive" regions in the positive view. It can be seen that the negative florbetapir retained its skeletal white matter profile and the coronal "M", while the white matter of the phantom (subjectively) approached the appearance of the positive scans. If the phantom is intended to be negative and only the cortical strip is evaluated rather than white matter "extent", then the difference in profile may not matter, if documented."

(9) Reference region: Greg Klein suggested adding a large uniform reference region, perhaps below the cerebellum.

(10) Visual versus SUVr interpretation. Dawn Mathews noted that

"It is the white matter "expansion", rather than any SUVR calculations, that caused the scan to appear "not negative" to me compared to florbetapir. ... from an SUVR standpoint, and visual read of the sagittal slices, typical regions did not appear positive, though occipital cortex did visually. In either case, a reference indicating what the white/gray boundaries were intended to be (which may have been exactly where the contrast boundaries were, if intended to be negative), would be useful."

(11) Quantitative comparisons: Dawn Mathews provided the following analysis [edited].

For the purpose of noting similarities and differences for plausibility, comparative images are provided below including: phantom, unsmoothed; phantom, smoothed; amyloid positive florbetapir scan SUVR 1.27, amyloid positive florbetapir scan SUVR 1.53, amyloid negative florbetapir scan, SUVR 0.96, SUVRs referenced to whole cerebellum. These scans are not spatially normalized to one another. Two different transaxial slices are shown (the second for phantom and amyloid negative scan only).

General: Yes, the phantom does not appear amyloid negative. Most telling is the expansion of uptake beyond typical white matter boundaries in the transaxial views (Figures 13 and 15). See notes below regarding whether pattern appears to be a typical positive scan or not.

Gray/white contrast: It appears to be most like florbetapir (high white uptake, minimal striatal binding in contrast to PiB).

Differences from typical amyloid positive images if the phantom were modeled after florbetapir:

- There is a noticeable visual difference in the degree of uptake in pons, whether positive or negative: little to moderate uptake in the phantom, but significantly more in the florbetapir scans.

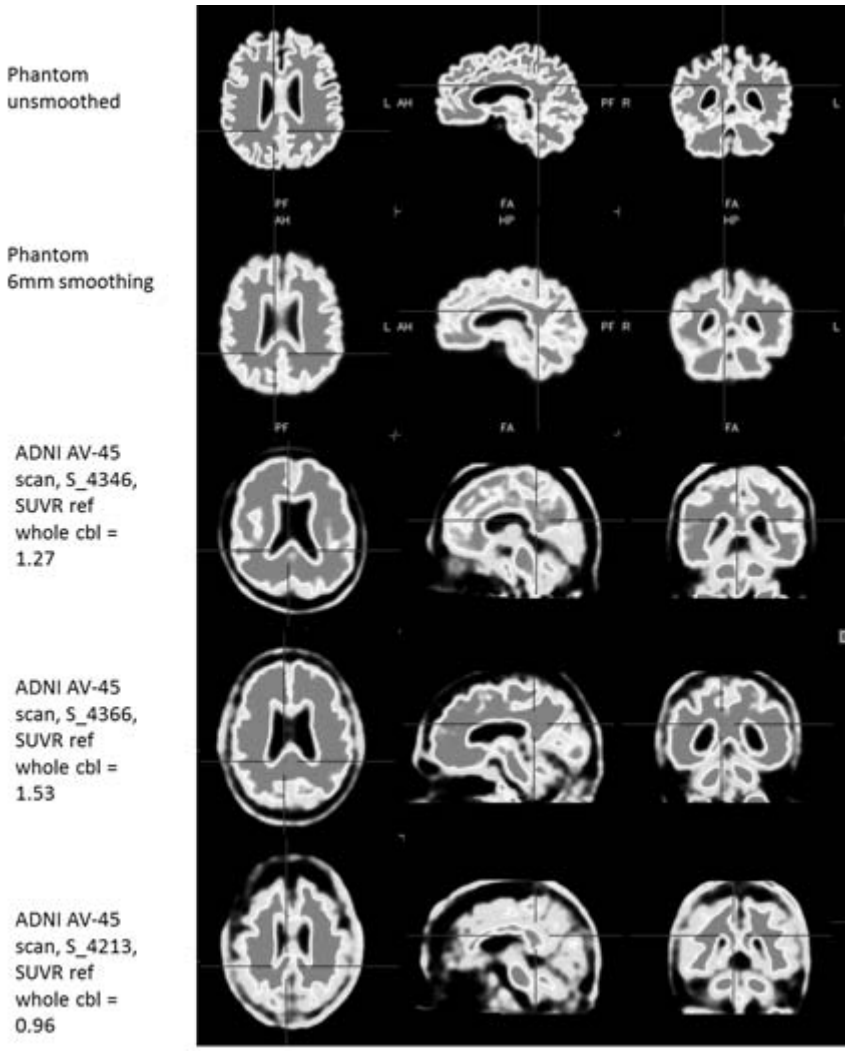

Figure 13. Comparison of phantom and AV-45 scans, positive and negative.

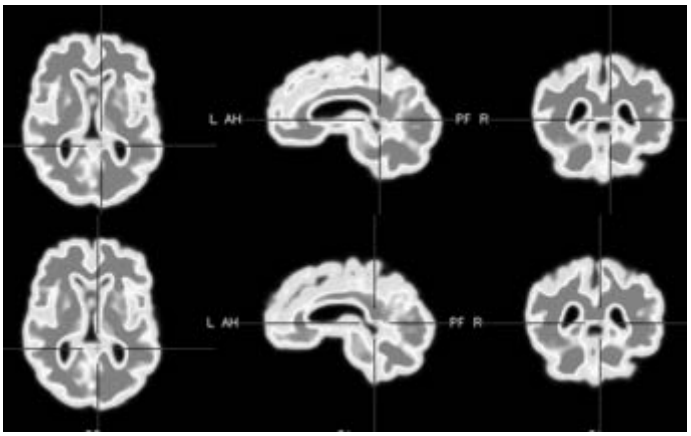

Figure 14. After lowering intensity threshold, and at two different sagittal slices.

- The cerebellum appears to have more signal in gray regions than typical amyloid scans. I think this was by design but indicates that SUVR measurements using cerebellum (and any region in this phantom) require a guide for translation to SUVR values using commercial tracers.

- As can be seen in the amyloid positive examples below, the phantom pattern differs from typical patterns but that may be by design. Whereas scans often show primary burden in posterior cingulate, precuneus, inferior frontal cortex and anterior cingulate, with minimal uptake until later on in occipital cortex, the phantom has as much if not more signal in occipital cortex. This may be desirable and intended for purposes of evaluating scanner output and processing output throughout the brain.

- Depending on how "positive" the scan is intended to be, I would have expected more signal to be visible in the sagittal view, including after smoothing (Figures 13 and 14). It is again the occipital cortex, using two different sagittal slices, that appears most positive but it is not clear to what extent the white matter encroaches medially to cause this.

- For the purposes of characterizing scanners and their white/gray contrast ratios as well as resolution and spillover effects, the above differences would not seem to matter.

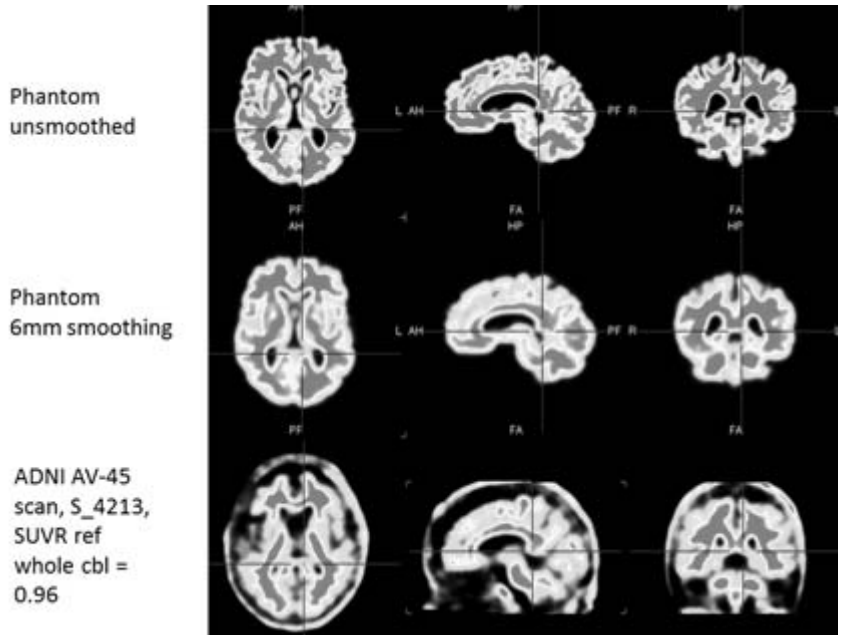

Figure 15. Comparison of phantom and amyloid negative scan, different sagittal slice.

Summary

The PET Amyloid DRO was completed and was evaluated by four experts. The unanimous consent was that the DRO provides a realistic appearance of a PET brain image of amyloid binding radiotracer, as well as ground truth information for evaluation of image analysis software. There is, however, room for improvement as noted above.

Potential Future Directions

(1) Due to the complexities of converting a reference MRI imaging to a PET amyloid binding radiotracer image, some adjustments and corrections should be made in a future version of the PET Amyloid DRO.

(2) The PET image should be accompanied with corresponding CT and MRI images.

(3) The radiotracer concentration and biodistribution should be adjustable to model different PET-amyloid imaging agents.

(4) Due to the project evolution, there are now small differences between the underlying structures of the PET Amyloid DRO and the template used for the physical phantom. These should be merged in a future version of the PET Amyloid DRO.

(5) Since we now have IRB-approved access to roughly 250 de-identified high-resolution MRI series of patients with known or suspected Alzheimer's disease or other dementias with comparable brain anatomies, it would be feasible to construct a library of PET Amyloid DROs with different characteristics.

Acknowledements

We want to thank in particular the reviewers Anne Smith (Siemens), Dawn Matthews (ADM Diagnostics, LLC), Greg Klein (BioClinica, Inc.), and David Lewis (University of Washington). We also thank the members of the QIBA Amyloid PET Biomarker Committee for helpful discussions and the RSNA staff for their continuing support of these activities.

Various QIBA projects and activities have been funded in whole or in part with Federal funds from the National Institute of Biomedical Imaging and Bioengineering, National Institutes of Health, Department of Health and Human Services, under Contract No. HHSN286201300071C.

References

(1) M. Azab, M. Carone, S. H. Ying, and D. M. Yousem, "Mesial Temporal Sclerosis: Accuracy of NeuroQuant versus Neuroradiologist.," AJNR Am J Neuroradiol, vol. 36, no. 8, pp. 1400–1406, Aug. 2015.

(2) DL Collins, AP Zijdenbos, V Kollokian, JG Sled, NJ Kabani, CJ Holmes and AC Evans. Design and Construction of a Realistic Digital Brain Phantom, IEEE Transactions on Medical Imaging, vol.17, No.3, p.463--468, June 1998.

(3) C. R. Jack, D. S. Knopman, W. J. Jagust, R. C. Petersen, M. W. Weiner, P. S. Aisen, L. M. Shaw, P. Vemuri, H. J. Wiste, S. D. Weigand, T. G. Lesnick, V. S. Pankratz, M. C. Donohue, and J. Q. Trojanowski, "Tracking pathophysiological processes in Alzheimer's disease: an updated hypothetical model of dynamic biomarkers.," Lancet Neurol, vol. 12, no. 2, pp. 207–216, Feb. 2013.

(4) S. Minoshima, "Establishing Amyloid PET Imaging Biomarkers: Ongoing Efforts.," AJNR Am J Neuroradiol, vol. 36, no. 7, pp. 1245–1246, Jul. 2015.

(5) L. A. Pierce, B. F. Elston, D. A. Clunie, D. Nelson, and P. E. Kinahan, “A Digital Reference Object to Analyze Calculation Accuracy of PET Standardized Uptake Value.,” Radiology, p. 141262, May 2015.

(6) S. D. Wollenweber, “A Multi-Contrast, Multi-Resolution Phantom for Radionuclide Imaging Using a Single Activity Concentration Fill,” IEEE Transactions on Nuclear Science, vol. 61, pp. 2503–2509, Oct. 2014.